Multiplicative resonant enhancement of chemical detection

Wenchao Ma,[1] Raphaël Pestourie,[2] Zin Lin,[3] Alan Aguirre-Soto,[4] Hadley D. Sikes,[5] and Steven G. Johnson[6,*]

[1] *Department of Chemistry, Massachusetts Institute of Technology, Cambridge, Massachusetts 02139, USA*
[2] *School of Computational Science and Engineering, Georgia Institute of Technology, Atlanta, Georgia 30332, USA*
[3] *Bradley Department of Electrical and Computer Engineering, Virginia Tech, Blacksburg, Virginia 24061, USA*
[4] *School of Engineering and Sciences, Tecnologico de Monterrey, Monterrey, Nuevo Leon 64849, Mexico*
[5] *Department of Chemical Engineering, Massachusetts Institute of Technology, Cambridge, Massachusetts 02139, USA*
[6] *Department of Mathematics, Massachusetts Institute of Technology, Cambridge, Massachusetts 02139, USA*

(Received 6 August 2024; revised 24 September 2024; accepted 2 October 2024; published 4 November 2024)

Optical resonances can increase the sensitivity of measurements to material perturbations and also accelerate photochemical reactions. Here, we show that these two effects can be combined *multiplicatively*, to enhance the detection via weak or low-concentration photochemical reactions far beyond what could previously be attained. For an optical resonance with quality factor Q, the sensitivity of our detection scheme is enhanced by $\sim Q^2$ (where $\sim$ denotes approximate proportionality), as demonstrated by both theoretical arguments and numerical simulations of a simple optical-grating resonance coupled with reaction-diffusion equations. Such an approach opens a door to further improvements by careful design of the resonance: even a three-parameter optimization of the grating resonance yields an additional $\approx$7 times improvement.

DOI: 10.1103/PhysRevApplied.22.054006

I. INTRODUCTION

We propose a chemical-sensing technique that exploits an optical resonance to *both* promote a photochemical reaction *and* detect a chemical (via resonance shift and hence transmission change) and show that detection sensitivity is enhanced by a factor of $\sim Q^2$, where Q is the quality factor [1,2] ($\sim$ lifetime $\sim$ 1/line width) of the resonance. In contrast, in conventional resonance-based schemes for chemical sensing or photochemistry, optical resonance is typically exploited to *either* sensitize response to material perturbation [3–7] *or* accelerate a reaction [8,9], whereas these effects can be multiplicative *if* the detection scheme is designed for it. In the simplest cases (for reaction rates that scale $\sim$ with the light intensity), each effect scales as $\sim Q$, so we obtain an overall $\sim Q^2$ enhancement. We study this $\sim Q^2$ dependence analytically with coupled-mode theory [10] and perturbation theory [11–13] and confirm the predictions with full-wave simulations in which Maxwell's equations are coupled with reaction-diffusion equations. The effect is illustrated in an etched dielectric grating resonator, which should be readily manufacturable. We also obtain another factor of $\approx$7 in sensitivity enhancement by numerically optimizing the grating parameters. (For a given Q, one can choose different resonant structures to maximize sensitivity and even higher performance may be attainable.) The $\sim Q^2$ enhancement occurs asymptotically for high Q in the regime of slow photochemical reactions and low concentrations of analytes (a regime in which enhancement is more needed); but large enhancements should persist qualitatively even at lower Q with faster photochemical reactions and higher concentrations of analytes. For purposes of illustration, we employ a simple reaction in which a reactant transforms reversibly to a product, but similar principles also apply to more complex reactions, as detailed in Appendix B. We also discuss analogies to nonlinear optical processes that exhibit $\sim Q^2$ enhancement, including Kerr [14] and Raman [15] effects.

II. THEORY

Let us begin with the essential ingredients of our detection scheme as depicted in Fig. 1, deferring mathematical details until later. We have a photochemical reaction with its reaction rate proportional to an optical intensity (e.g., in a single-photon absorption process [16]). In a low-loss optical resonant cavity, the electric-field energy

*Contact author: stevenj@math.mit.edu

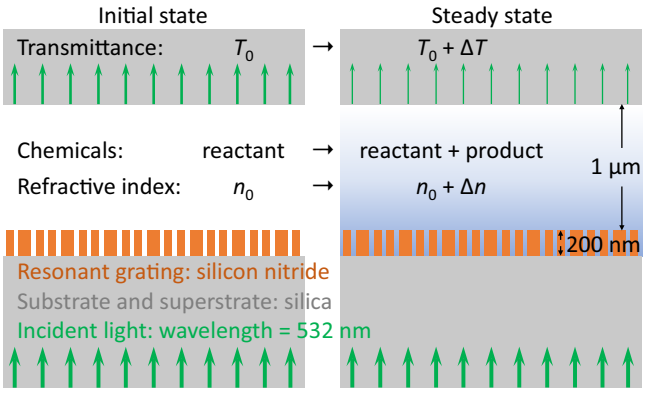

FIG. 1. A schematic of the detection scheme with example geometry: incident light induces a photochemical reaction, causing a change Δn in the refractive index of the solution, detected by a change ΔT in light transmission. If the reaction occurs near an optical resonance, e.g., in a microfluidic channel, *multiplicative* resonant enhancement of the detection sensitivity may be enabled. Here, we show a simple resonant structure formed from a dielectric grating on a low-index substrate, where the precise grating parameters are determined by the desired quality factor Q and resonant frequency ω_0, here for wavelength ≈532 nm as an example.

density $|E|^2$ ("intensity" hereafter) is proportional to Q (with all other influences being fixed) [10], so the equilibrium concentration of the photoactivated chemical grows with $\sim Q$ in a regime in which the reagent is far from being exhausted. The reaction product typically has a different refractive index from the reactant even at the same concentration [17]. The reaction will cause an index shift Δn proportional to a small concentration change [1,18] and hence Δn scales as $\sim Q$. This change will shift the resonance frequency ω_0 by $\Delta\omega_0 \sim \Delta n$ [11–13], corresponding to shift of a sharp peak of a Fano resonance [10] in the transmission or reflection spectrum. Because the line width of this peak scales as $\sim 1/Q$, the slope $d(\text{power})/d\omega_0$ around the resonant frequency ω_0 scales as $\sim Q$. Consequently, the transmitted power in the vicinity of a shifted peak will change by $\sim \Delta\omega_0\, d(\text{power})/d\omega_0 \sim \Delta n\, d(\text{power})/d\omega_0 \sim Q^2$. (Like any resonant enhancement [11], this scaling holds until Q approaches the limit imposed by intrinsic losses such as absorption, as quantified in Appendix A.)

To illustrate the enhancement, we investigate a model reaction process (greatly generalized in Appendix B):

$$\text{reactant} \underset{}{\overset{h\nu}{\rightleftharpoons}} \text{product} \tag{1}$$

The reactant is the analyte, namely, the target chemical being detected. The forward reaction is induced by light. For monochromatic illumination at a frequency ω, the rate constant k_0 (spatially varying) of the forward reaction is proportional to the local light intensity $|E|^2$ at a location $\mathbf{x}$:

$$k_0(\mathbf{x}) \sim |E(\mathbf{x}, \omega)|^2. \tag{2}$$

Hereafter, we assume monochromatic illumination and mostly omit the arguments $\mathbf{x}$ and ω. Our backward reaction is not influenced by light, with a uniform rate constant k_1. Both the reactant and the product are dissolved in solvent, with concentrations c_0 and c_1 and diffusion coefficients D_0 and D_1, respectively. In the solution region, c_0 and c_1 can vary with the location but we assume D_0 and D_1 to be uniform. Both the forward and backward reactions are first order (rate ∼ concentration). This reaction-diffusion system evolves with time t as [19]

$$\begin{aligned} \frac{\partial c_0}{\partial t} &= D_0 \nabla^2 c_0 - k_0 c_0 + k_1 c_1, \\ \frac{\partial c_1}{\partial t} &= D_1 \nabla^2 c_1 + k_0 c_0 - k_1 c_1. \end{aligned} \tag{3}$$

(A more general system involving an arbitrary number of reactions is analyzed in Appendix B: mathematically, the basic requirement for multiplicative resonant enhancement turns out to be that the first-order photochemically induced change in the refractive index occurs only in the presence of the analyte.) We assume that the illumination turns on at $t = 0$, before which $k_0 = 0$ is guaranteed and only the reactant is present. At equilibrium (where $\partial c_0/\partial t = \partial c_1/\partial t = 0$), concentrations have a nonlinear dependence on k_0, but in this work, we focus on the weak-reaction regime $k_0 \ll k_1$, in which resonant enhancement is more useful. This regime allows us to linearize the equilibrium solution in the photochemical reaction rate k_0:

$$\frac{c_1^{\text{eq}}}{\langle c \rangle} \approx (k_1 - D_1 \nabla^2)^{-1} k_0, \tag{4}$$

where $c = c_0|_{t=0}$ is the initial concentration of the reactant and the angle brackets denote a spatial average. We drop the superscript for equilibrium hereafter. For illustration, we take c to be uniform in space, so that c is also the analytical concentration of the analyte [20,21]; we set $D_0 = D_1 = D$ here but the same scaling is obtained for heterogeneous conditions (as discussed in Appendix B). This linearization in Eq. (4) simplifies the analysis and eliminates some dimensionful parameters (such as the incident light irradiance and the ratio of k_0 to $|E|^2$) from the final enhancement factor. Furthermore, for a dilute solution or a reaction that has proceeded to a small extent, the refractive-index change due to the reaction will be approximately linear in the product concentration:

$$\Delta n(\mathbf{x}) \sim c_1(\mathbf{x}), \tag{5}$$

where Δn (spatially varying) is the difference between the equilibrium and initial refractive indices of the solution.

Since intensity enhancement is most pronounced inside and near the resonant cavity, we consider an optofluidic microsystem in which the solution is spatially confined by, e.g., a fluidic microchannel or a thin fluid film [22–24] (neglecting convection), as exemplified in Fig. 1. Light induces the forward reaction, drives a tiny portion of reactant to product, perturbs the refractive index of the solution, and hence alters the transmittance T (the ratio of transmitted to incident power). The sensitivity S of detection is defined as the derivative of the transmission change ΔT (between equilibrium and initial states) with respect to the initial analyte concentration c, scaled by the fluid volume V (so that cV is the amount of the analyte), evaluated as $c \to 0^+$:

$$S = \frac{1}{V}\frac{\partial \Delta T}{\partial c}\bigg|_{c\to 0^+} = \frac{1}{V}\int_\Omega \frac{\partial \Delta T}{\partial \Delta n}\frac{\partial \Delta n}{\partial c}\bigg|_{c\to 0^+} dv$$
$$= \frac{1}{V}\int_\Omega \frac{\partial T}{\partial n}\frac{\Delta n}{c}\bigg|_{c\to 0^+} dv, \tag{6}$$

where Ω is the fluid region and dv is the volume element in three dimensions (3D) or the area element in two dimensions (2D). Hereafter, both S and $|S|$ are referred to as sensitivity; all the derivatives are always evaluated as $c \to 0^+$ and we omit the subscript.

Resonance enhances both $\partial T/\partial n$ and Δn in Eq. (6) and hence the sensitivity. The factor $\partial T/\partial n$ can be decomposed as $(\partial T/\partial\omega_0)(\partial\omega_0/\partial n)$, where ω_0 is the resonant frequency. According to coupled-mode theory [10,25–27], both $\partial T/\partial\omega_0$ and $|E|^2$ near $\omega = \omega_0$ scale as $\sim Q$ if other factors are fixed and intrinsic loss is negligible compared with the loss due to radiative coupling. On the other hand, perturbation theory indicates that the resonant-frequency shift due to an index perturbation satisfies $\Delta\omega_0 \sim \Delta n$ to first order [11–13], which also scales as $\sim Q$ due to Eqs. (2), (4) and (5). Therefore, the sensitivity scales as $\sim Q^2$:

$$S \sim \frac{\partial T}{\partial\omega_0}\frac{\partial\omega_0}{\partial n}\Delta n \sim \frac{\partial T}{\partial\omega_0}\Delta n \sim Q^2. \tag{7}$$

This discussion assumes detection uses a frequency ω close to ω_0 and with nonzero $\partial T/\partial\omega_0$ (close to, but not exactly at, maximum T). We show below that a slightly off-resonant frequency is usually optimal. (For a Lorentzian line shape, a slightly off-resonant frequency is required because $\partial T/\partial\omega_0$ vanishes at $\omega = \omega_0$.) In Appendix C 2, we show a similar $\sim Q^2$ enhancement in a more general system, even when the analyte does not directly participate in the photochemical reaction.

III. NUMERICAL VERIFICATION

To concretely demonstrate the scaling, we consider a set of resonators with similar shapes and mode profiles but vastly different quality factors (Q), which are constructed by small perturbations to a high-Q resonator [28];

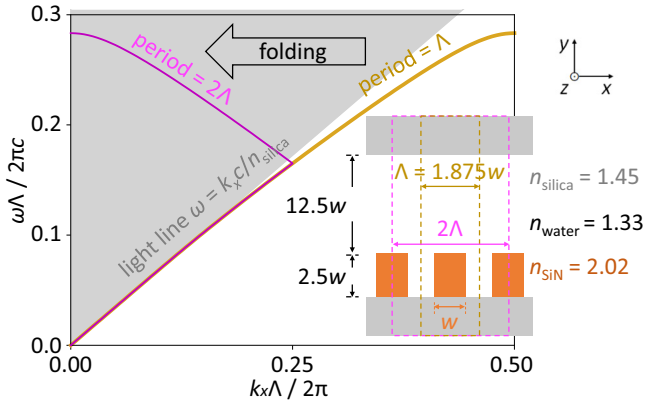

FIG. 2. The starting point for our example structure: the geometry (inset) and guided-mode dispersion relation of an unperturbed period-Λ dielectric grating. The fundamental E_z-polarized guided mode (yellow curve) is "folded" back to $k_x = 0$ (magenta curve) if the period is doubled to a period-2Λ supercell. This folded band becomes leaky if the ridge widths are perturbed to break the Λ periodicity.

many such structures exist, often thought of as perturbed "bound-in-continuum" modes [29,30]. We start with a period-Λ grating of silicon nitride ridges, as shown in Fig. 2 with the dispersion relation of its guided mode [11] for the out-of-plane (E_z) polarization (computed by free planewave-expansion software [31]). If one considers a period-2Λ supercell, the corresponding guided band (magenta curve) is artificially "folded" back [11] into the light cone (the spectrum of radiating modes) and at $k_x = 0$ can be viewed as an infinite-Q standing-wave resonance. To obtain a finite-Q resonance that couples to or from normal-incidence radiation ($k_x = 0$), one can simply break the Λ periodicity by perturbing the equal-width ridges into an alternation between slightly wider and narrower ridges [28], so that 2Λ becomes the minimal period. As shown in Fig. 3, with the width perturbation $\pm 2\delta$, the resulting Q for $k_x = 0$ scales as δ^{-2} [28,32] (which also follows from perturbation theory: the scattered power scales as the square of the volume of the perturbation [33]). (This and subsequent electromagnetic simulations are performed with a free-software implementation of the finite-difference time-domain method [34].) This small perturbation yields a family of resonators that essentially differ only in Q, so that the reaction-diffusion equations change only by approximately an overall scale factor in $k_0 \sim |E|^2$.

As shown in the upper-right inset of Fig. 3, around the resonant frequency ω_0, transmission through such a high-Q resonator exhibits a Fano-resonance line shape [10,35], which is typically sharp and asymmetric, with the transmittance varying substantially over a narrow frequency range on the scale of ω_0/Q. Asymptotically, the slope of the transmission spectrum at ω_0 is proportional to Q [10], as in our analysis for Eq. (7).

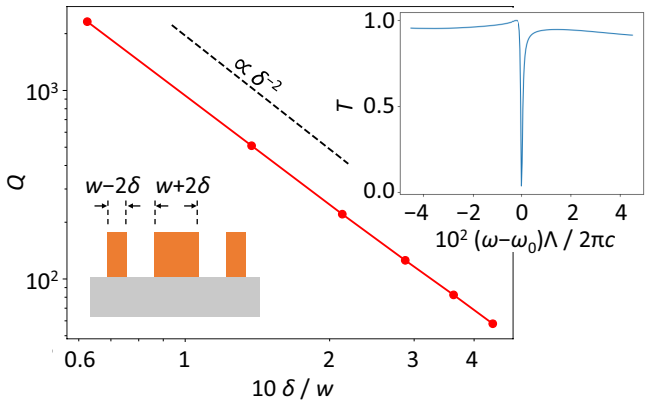

FIG. 3. Controlling the resonance lifetime in our example structure: alternating $\pm 2\delta$ perturbations to the ridge widths (left inset) doubles the period and leads to Q (red dots and solid line) $\sim 1/\delta^2$ (dashed line), diverging to an infinite-Q guided mode as $\delta \to 0$ [28]. One can thus change Q while keeping the geometry and the intensity profile nearly fixed. The right inset shows the Fano-resonance line shape of the transmittance T around $\omega = \omega_0$ at $Q = 667$, with a slope $dT/d\omega_0 \sim Q$ near $\omega = \omega_0$.

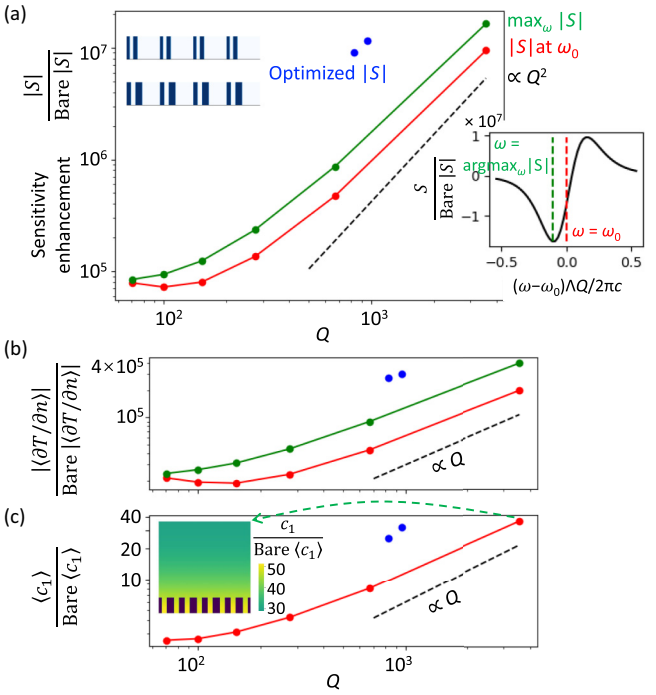

FIG. 4. (a) The computed detection sensitivity $|S|$ for our example structure as a function of Q, normalized by the value for a bare surface (no grating), at both the resonant frequency ω_0 (red dots) and the frequency of maximum $|S|$ (green dots), with the corresponding frequencies labeled on $S(\omega)$ (for $Q = 667$) as dashed lines (right inset). Also illustrated are the sensitivities (blue dots) of two optimized grating structures (blue insets) at different Q values. The observed $\sim Q^2$ dependence (asymptotically parallel to the dashed-line Q^2 reference) arises from a product of two $\sim Q$ enhancements shown below (with dashed-line Q references): (b) the magnitude of the mean sensitivity of the measurements to small changes in refractive index, namely, $|\langle dT/dn\rangle|$, scales as $\sim Q$ near ω_0 due to the steep slope of T, where the lower (red) and upper (green) curves are evaluated at ω_0 and argmax$_\omega|S|$; and (c) the mean concentration of the reaction product, namely, $\langle c_1\rangle$, scales as $\sim Q$ at ω_0 due to the resonant enhancement of the intensity. The inset of (c) depicts the normalized equilibrium concentration of the reaction product in a structure with $Q = 3565$, corresponding to the data point at the right end of the scaling curve. The dark rectangles denote the silicon nitride ridges, which cannot be occupied by the fluid. In (b) and (c), the blue dots correspond to the optimized cases, as in (a).

To demonstrate the proportionality relationship in Eq. (7) with our example grating structure, we plot simulated values of $|\langle\partial T/\partial n\rangle|$, $\langle c_1\rangle$, and $|S|$ at $\omega = \omega_0$ as functions of Q in Fig. 4, normalized by the corresponding quantities evaluated for a bare silica surface (no grating) at the same frequency. In this demonstration, we set $D\lambda_0^2/k_1 = 0.532^2$, where $\lambda_0 = 2\pi c/\omega_0$ is the wavelength. By rescaling the structure, one can set ω_0 to any desired frequency; e.g., for the unperturbed case ($\delta = 0$), the dispersion relation in Fig. 2 gives $\Lambda/\lambda_0 = 0.283$, so with $\lambda_0 = 532$ nm, one obtains $\Lambda = 151$ nm and $w = \Lambda/1.875 = 80$ nm. The simulation results exhibit our predicted asymptotic scaling relations $|\langle\partial T/\partial n\rangle| \sim Q$, $\langle c_1\rangle \sim Q$, and $|S| \sim Q^2$. Due to the enhanced intensity near the grating, the reaction product at equilibrium is more concentrated there, as illustrated in the inset of Fig. 4(c).

High-Q resonators are typically vulnerable to fabrication imperfections and hence resonators with high sensitivity $|S|$ at relatively low Q are preferred. For a given Q (determined by fabrication tolerances and the bandwidth of k_0), $|S|$ can be further increased by optimizing both the detuning $\omega - \omega_0$ and the structure itself. Similar to $\max_\omega |\partial T/\partial\omega_0|$ (as analytically calculated in Appendix A), $\max_\omega |S|$ often occurs slightly off resonance, as shown in the lower-right inset of Fig. 4(a), where $k_0/|E|^2$ is assumed to be uniform across the frequency range. Therefore, detuning the resonance ω_0 from the pump or probe frequency ω can be favorable. The dependence of $\max_\omega |S|$ still scales as $\sim Q^2$, as illustrated by the green curve in Fig. 4(a). One can also optimize the structure, since different geometries that attain the same Q are possible. For example, we have performed optimization of $|S|\,|_{\omega=\omega_0}/f\,(Q)$ by an evolution strategy that searches many local optima [36], where $f\,(Q)$ is interpolated and extrapolated from the data of $(Q, |S|\,|_{\omega=\omega_0})$ in the scaling curve from Fig. 4(a) in order to normalize out the effect of changes in Q (and thus to improve performance for that Q). The structure in a unit cell has been parametrized by the widths of the two ridges and of the gap between them. The values of $\max_\omega |S|$ of the optimized gratings are labeled as two blue dots, with four periods of those gratings illustrated in the upper-left inset of Fig. 4(a). Even this simple

three-parameter optimization increases $\max_\omega |S|$ by a factor of $\approx$7, compared to the previous $w \pm \delta$ structures at the same Q values.

IV. CONCLUSION

In this work, we have shown by both analytical arguments and numerical examples that chemical detection can be enhanced multiplicatively by the same resonance to increase both the reaction rate and the sensitivity of measurements to material perturbations. Our numerical example is in the context of a particular toy model, but the basic principle is more generally applicable as discussed in Appendix B and further generalizations may be possible (e.g., to high-concentration or time-dependent regimes in which some figure of merit other than linearized sensitivity will be required). In practice, the detection can utilize a range of frequencies near resonance instead of a single frequency, and picosecond or femtosecond optics may be required for some fast chemical processes. Our scheme may be more beneficial to the detection involving vulnerable chemical species, which may easily suffer from side reactions due to light or heat and hence need weak illumination. Potential photochemical candidates to explore with this mechanism may include photoisomerization reactions [37], photo-Fries rearrangements [38], the formation of polymer brushes by photo–atom transfer radical polymerization (ATRP) [39], and the photodimerization of pendant groups in polymers [40]. Reactions with large refractive-index contrast between the reactant and product have been studied [41] and would be especially suitable for our detection scheme. Although the chemicals are dissolved in fluid in our toy model, a similar resonant enhancement should still appear in solid-phase reactions [42,43] (which lack only the diffusion terms). We also note that analogous multiplicative resonant enhancement occurs in nonlinear optical systems, such as $\sim Q^2$ power reduction in optical bistability from Kerr nonlinearities [44] or $\sim Q^2$ enhancement of Raman sensing via surface plasmons [45]. Considerable effort has been expended in maximizing Kerr [46] and surface-enhanced Raman scattering (SERS) [47–49] effects, and similar improvements in chemical sensing seem ripe for future exploitation.

ACKNOWLEDGMENTS

This work was supported in part by the U.S. Army Research Office through the Institute for Soldier Nanotechnologies (Award No. W911NF-23-2-0121) and by the Simons Foundation.

APPENDIX A: TEMPORAL COUPLED-MODE THEORY AND FANO-RESONANCE LINE SHAPE

Interference between a direct pathway and a resonance-mediated indirect pathway typically exhibits a sharp asymmetric line shape in optical transmission and reflection spectra. Such a line shape is often termed the Fano-resonance line shape. In this appendix, we briefly review the temporal coupled-mode theory, derive the Fano-resonance line shape for a lossless two-port structure, similar to previous work [10], and also discuss the effect of intrinsic loss [29]. From these equations, one can see explicitly that the field intensity of the resonant mode scales proportional to Q and also that the transmission slope $dT/d\omega$ scales proportional to Q in the vicinity of the resonance frequency.

Consider a single-mode optical resonator coupled with m ports [10]. The dynamics of the amplitude a of the resonant mode can be described as

$$\frac{da}{dt} = \left(i\omega_0 - \frac{1}{\tau}\right) a + \boldsymbol{\kappa}^\top \mathbf{s}_+, \quad \mathbf{s}_- = C\mathbf{s}_+ + a\mathbf{d}, \tag{A1}$$

where ω_0 denotes the resonant frequency, τ denotes the lifetime of resonance that is proportional to the quality factor $Q = \omega_0\tau/2$, and t denotes the time variable. The incoming and outgoing waves are denoted by $\mathbf{s}_+$ and $\mathbf{s}_-$, respectively. The coupling between $\mathbf{s}_+$ and the resonant mode is denoted as $\boldsymbol{\kappa}$. The coupling between $\mathbf{s}_-$ and the resonant mode is denoted as $\mathbf{d}$. For a system with two or more ports, $\mathbf{s}_+$, $\mathbf{s}_-$, $\boldsymbol{\kappa}$, and $\mathbf{d}$ can be written as column vectors, each of which has m elements with $m \geq 2$. The $m \times m$ matrix C is the scattering matrix of the direct pathway. If multiple loss channels are present, the overall decay rate $1/\tau$ should be understood as the sum of the decay rates of all channels. The overall scattering matrix S is

$$S = C + \frac{\mathbf{d}\boldsymbol{\kappa}^\top}{1/\tau + i(\omega - \omega_0)}, \tag{A2}$$

which operates as $\mathbf{s}_- = S\mathbf{s}_+$. The amplitude of the resonant mode is

$$a = \frac{\boldsymbol{\kappa}^\top \mathbf{s}_+}{1/\tau + i(\omega - \omega_0)}. \tag{A3}$$

For a lossless reciprocal system, the conservation of energy and time-reversal symmetry impose constraints as [10,25,39]

$$\boldsymbol{\kappa} = \mathbf{d}, \tag{A4a}$$

$$C\mathbf{d}^* = -\mathbf{d}, \tag{A4b}$$

$$\mathbf{d}^\dagger \mathbf{d} = \frac{2}{\tau}, \tag{A4c}$$

$$C^\top = C, \quad C^\dagger C = \mathbb{1}, \tag{A4d}$$

where $\mathbb{1}$ is the identity matrix. The relations in Eqs. (A4a), (A4b), and (A4c) and the unitarity of C in Eq. (A4d)

enforce the overall scattering matrix S in Eq. (A2) to be unitary, namely, $S^\dagger S = \mathbb{1}$. The relation in Eq. (A4a) and the symmetry of C in Eq. (A4d) enforce S to be symmetric, namely, $S^\top = S$.

The governing equations in Eq. (A1) are invariant if the matrix and vectors undergo transformations simultaneously as

$$\begin{aligned} &\mathbf{s}_+ \to U^*\mathbf{s}_+, \quad \mathbf{s}_- \to U\mathbf{s}_-, \\ &\boldsymbol{\kappa} \to U\boldsymbol{\kappa}, \quad \mathbf{d} \to U\mathbf{d}, \\ &C \to UCU, \end{aligned} \tag{A5}$$

where U is a unitary and symmetric matrix. This freedom allows C to be simplified. For a two-port lossless structure, the general form of the scattering matrix can be written as

$$C_{\text{general}} = e^{i\zeta}\begin{pmatrix} e^{i\phi}\cdot r & t \\ t & -e^{-i\phi}\cdot r \end{pmatrix}, \tag{A6}$$

where r and t are real numbers satisfying

$$r^2 + t^2 = 1. \tag{A7}$$

(Here and hereafter, t is a parameter in the scattering matrix and no longer the time variable.) The phase factors can be canceled by Eq. (A5), with

$$U = e^{-i\zeta/2}\begin{pmatrix} e^{-i\phi/2} & 0 \\ 0 & ie^{i\phi/2} \end{pmatrix}, \tag{A8}$$

which results in

$$C = UC_{\text{general}}U = \begin{pmatrix} r & it \\ it & r \end{pmatrix}. \tag{A9}$$

According to Eqs. (A4b) and (A9), the components of $\mathbf{d}$, denoted by $d_1 = |d_1|e^{i\theta_1}$ and $d_2 = |d_2|e^{i\theta_2}$ with $\theta_1, \theta_2 \in \mathbb{R}$, should satisfy

$$\begin{aligned} (r+1)|d_1|\cos\theta_1 &= -t|d_2|\sin\theta_2, \\ (r-1)|d_1|\sin\theta_1 &= t|d_2|\cos\theta_2. \end{aligned} \tag{A10}$$

From Eqs. (A4c), (A7), and (A10), one can obtain

$$|d_1||d_2|\sin(\theta_1+\theta_2) = -\frac{t}{\tau}. \tag{A11}$$

If the resonance decays into the two ports with lifetimes τ_1 and τ_2, one has

$$|d_1| = \sqrt{\frac{2}{\tau_1}}, \quad |d_2| = \sqrt{\frac{2}{\tau_2}}, \quad \frac{1}{\tau_1} + \frac{1}{\tau_2} = \frac{1}{\tau}. \tag{A12}$$

As implied by Eqs. (A11) and (A12), the parameters satisfy [35]

$$|t| \le \frac{2}{\sqrt{\tau_1/\tau_2} + \sqrt{\tau_2/\tau_1}} = \sqrt{1-\eta^2} \tag{A13}$$

or, equivalently,

$$|r| \ge |\eta|, \tag{A14}$$

where η quantifies the relative difference between the two decay rates or lifetimes:

$$\eta = \frac{1/\tau_1 - 1/\tau_2}{1/\tau_1 + 1/\tau_2} = \frac{\tau_2 - \tau_1}{\tau_1 + \tau_2}. \tag{A15}$$

[The inequalities in Eqs. (A13) and (A14) become trivial for symmetrical decay rates $\tau_1 = \tau_2$ or for $|r| = 1$.] From Eqs. (A7), (A11), and (A12), one can obtain

$$|d_1||d_2|\cos(\theta_1+\theta_2) = \pm\frac{1}{\tau}\sqrt{r^2-\eta^2}. \tag{A16}$$

According to Eqs. (A2), (A11), and (A16), the off-diagonal element of the scattering matrix S is

$$\begin{aligned} S_{12} = S_{21} &= it + \frac{|d_1||d_2|e^{i(\theta_1+\theta_2)}}{1/\tau + i(\omega-\omega_0)} \\ &= \frac{\pm\sqrt{r^2-\eta^2}/\tau - t(\omega-\omega_0)}{1/\tau + i(\omega-\omega_0)}, \end{aligned} \tag{A17}$$

The transmittance is

$$\begin{aligned} T &= \frac{|s_{2-}|^2}{|s_{1+}|^2} = |S_{21}|^2 \\ &= \frac{t^2(\omega-\omega_0)^2 + (r^2-\eta^2)/\tau^2 \mp 2t(\omega-\omega_0)\sqrt{r^2-\eta^2}/\tau}{(\omega-\omega_0)^2 + 1/\tau^2}, \end{aligned} \tag{A18}$$

where s_{1+} denotes the first component of $\mathbf{s}_+$ and s_{2-} denotes the second component of $\mathbf{s}_-$. The reflectance is $R = 1 - T$.

The transmission spectrum in Eq. (A18) has several properties. The slope of the transmission spectrum at the resonant frequency ω_0 is

$$\left.\frac{\partial T}{\partial\omega}\right|_{\omega=\omega_0} = -\left.\frac{\partial T}{\partial\omega_0}\right|_{\omega=\omega_0} = 2\tau t\sqrt{r^2-\eta^2}. \tag{A19}$$

The maximum unsigned slope is

$$\begin{aligned} \max_\omega\left|\frac{\partial T}{\partial\omega}\right| &= \max_\omega\left|\frac{\partial T}{\partial\omega_0}\right| \\ &= \tau(1-\eta^2)\sin^3\left[\frac{2}{3}\arccos\left(-\sqrt{\frac{r^2-\eta^2}{1-\eta^2}}\right)\right], \end{aligned} \tag{A20}$$

which is attained at

$$\underset{\omega}{\operatorname{argmax}}\left|\frac{\partial T}{\partial \omega}\right| = \omega_0 \mp \frac{\operatorname{sgn}(t)}{\tau}\cot\left[\frac{2}{3}\arccos\left(-\sqrt{\frac{r^2-\eta^2}{1-\eta^2}}\right)\right]. \tag{A21}$$

These two characteristic slopes are proportional to τ or Q, if r and τ_1/τ_2 do not change with τ while r and η satisfy $|\eta| < |r| < 1$. The ratio between the two slopes is

$$\left|\frac{\partial T}{\partial \omega}\right|_{\omega=\omega_0} \Big/ \max_{\omega}\left|\frac{\partial T}{\partial \omega}\right| = 4 - 3\csc^2\left[\frac{2}{3}\arccos\left(-\sqrt{\frac{r^2-\eta^2}{1-\eta^2}}\right)\right]. \tag{A22}$$

The corresponding transmittance is

$$\begin{aligned} &T(\omega=\omega_0) = r^2-\eta^2, \\ &T\left(\omega = \underset{\omega}{\operatorname{argmax}}\left|\frac{\partial T}{\partial \omega}\right|\right) = (1-\eta^2)\sin^2\left[\frac{1}{3}\arccos\left(-\sqrt{\frac{r^2-\eta^2}{1-\eta^2}}\right)\right]. \end{aligned} \tag{A23}$$

The extrema of transmittance are

$$\max_{\omega} T = 1-\eta^2, \quad \min_{\omega} T = 0, \tag{A24}$$

which are attained at

$$\begin{aligned} &\underset{\omega}{\operatorname{argmax}}\, T = \omega_0 \mp \frac{t}{\tau\sqrt{r^2-\eta^2}}, \\ &\underset{\omega}{\operatorname{argmin}}\, T = \omega_0 \pm \frac{\sqrt{r^2-\eta^2}}{\tau t}. \end{aligned} \tag{A25}$$

The line shape in Eq. (A18) reduces to Lorentzian at either $|r| = |\eta|$ or $t = 0$. Due to the vanishing slope at ω_0, detuning the detection frequency from ω_0 is required. If both $|r| = |\eta|$ and $t = 0$ are satisfied, Eq. (A18) predicts no transmission.

According to Eqs. (A3), (A4a), and (A12), one can write the field intensity of the resonant mode as

$$|a|^2 = 2\frac{|s_{1+}|^2/\tau_1 + |s_{2+}|^2/\tau_2 + 2|s_{1+}|\,|s_{2+}|\cos\varphi/\sqrt{\tau_1\tau_2}}{(\omega-\omega_0)^2 + (1/\tau_1+1/\tau_2)^2}, \tag{A26}$$

where s_{1+} and s_{2+} are the components of $\mathbf{s}_+$ and φ is the argument difference between $\kappa_{1+}s_{1+}$ and $\kappa_{2+}s_{2+}$, with κ_{1+} and κ_{2+} denoting the components of $\boldsymbol{\kappa}$. If the incoming wave comes only from the first port, the intensity is

$$|a|^2 = \frac{2|s_{1+}|^2/\tau_1}{(\omega-\omega_0)^2 + (1/\tau_1+1/\tau_2)^2}. \tag{A27}$$

This intensity is approximately proportional to τ or Q at $\omega = \omega_0$ in a regime in which τ_2/τ_1 is nearly fixed, e.g., τ_1 and τ_2 increase at the same rate as τ increases. If τ_2/τ_1 is not fixed but $\tau_1 \ll \tau_2$ is satisfied, the intensity is also approximately proportional to τ or Q at $\omega = \omega_0$. In the opposite limit, where $\tau_1 \gg \tau_2$ holds, Eq. (A27) indicates $|a|^2 \approx 2|s_{1+}|^2\tau_2^2/\tau_1$ at $\omega = \omega_0$; if τ_2/τ_1 is not fixed in this case, the intensity does not scale as $\sim\tau$ or $\sim Q$. Both $\tau_1 \ll \tau_2$ and $\tau_1 \gg \tau_2$ rely on $t \approx 0$ according to Eq. (A13) and further cause $T \approx 0$.

For a lossy structure, the decay rate $1/\tau$ in Eq. (A1) should be understood as $1/\tau = 1/\tau_e + 1/\tau_i$, where τ_e is the lifetime associated with coupling to external ports, while τ_i is the lifetime associated with intrinsic losses such as absorption and leakage due to surface roughness, disorder in media, and finite-size effects [11,27,29]. The corresponding quality factors are $Q_e = \omega_0\tau_e/2$ and $Q_i = \omega_0\tau_i/2$. The overall lifetime is $\tau = \tau_e\tau_i/(\tau_e+\tau_i)$ and the overall quality factor is $Q = Q_eQ_i/(Q_e+Q_i)$. With $Q_e \gg 1$ and $Q_i \gg 1$, Eqs. (A4a), (A4b), and (A4d) remain unchanged but τ in Eq. (A4c) should be replaced by τ_e. The transmittance turns out to be

$$T = \frac{t^2[(\omega-\omega_0)^2 + 1/\tau_i^2] + (r^2-\eta^2)/\tau_e^2 \mp 2t(\omega-\omega_0)\sqrt{r^2-\eta^2}/\tau_e}{(\omega-\omega_0)^2 + (1/\tau_e+1/\tau_i)^2}. \tag{A28}$$

The slopes of T with respect to ω_0, $1/\tau_e$, and $1/\tau_i$ at $\omega = \omega_0$ are

$$\begin{aligned}
\left.\frac{\partial T}{\partial \omega_0}\right|_{\omega=\omega_0} &= -\left.\frac{\partial T}{\partial \omega}\right|_{\omega=\omega_0} = -2\frac{t\sqrt{r^2-\eta^2}/\tau_e}{(1/\tau_e+1/\tau_i)^2} \\
&= -2t\sqrt{r^2-\eta^2}\frac{\tau_e\tau_i^2}{(\tau_e+\tau_i)^2}, \\
\left.\frac{\partial T}{\partial (1/\tau_e)}\right|_{\omega=\omega_0} &= 2\frac{(r^2-\eta^2)/(\tau_e\tau_i) - t^2/\tau_i^2}{(1/\tau_e+1/\tau_i)^3} \\
&= 2\frac{(r^2-\eta^2)(\tau_e\tau_i)^2 - t^2\tau_i\tau_e^3}{(\tau_e+\tau_i)^3}, \\
\left.\frac{\partial T}{\partial (1/\tau_i)}\right|_{\omega=\omega_0} &= 2\frac{t^2/(\tau_e\tau_i) - (r^2-\eta^2)/\tau_e^2}{(1/\tau_e+1/\tau_i)^3} \\
&= 2\frac{(t\tau_e\tau_i)^2 - (r^2-\eta^2)\tau_e\tau_i^3}{(\tau_e+\tau_i)^3}.
\end{aligned} \tag{A29}$$

For $\tau_e \ll \tau_i$ with $|\eta| < |r| < 1$, the slopes with respect to ω_0 and $1/\tau_i$ are approximately proportional to $\tau_e \approx \tau$ or $Q_e \approx Q$, whereas the slope with respect to $1/\tau_e$ is negligible and vanishes in the absence of intrinsic loss. As the example in Fig. 5(a) shows, for $\tau_e \ll \tau_i$, the slopes $\partial T/\partial\omega_0$ and $\partial T/\partial(1/\tau_i)$ at $\omega = \omega_0$ scale linearly with τ_e or Q_e, while $\partial T/\partial(1/\tau_e)$ is negligible by comparison. In the regime with $\tau_e \gg \tau_i$, $\partial T/\partial\omega_0$ and $\partial T/\partial(1/\tau_i)$ approach zero, while $\partial T/\partial(1/\tau_e)$ reaches a plateau.

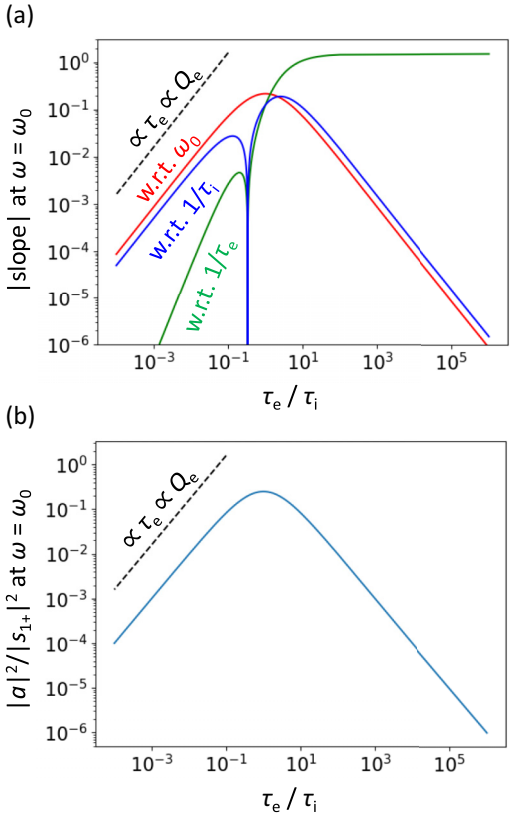

FIG. 5. The magnitudes of the slopes of the transmission spectrum and normalized mode intensities at the resonant frequency. We set $\tau_{e1} = \tau_{e2} = 2\tau_e$, $\tau_i = 1$, and $r = 0.5$ here. (a) $|\partial T/\partial\omega_0|$, $|\partial T/\partial(1/\tau_e)|$, and $|\partial T/\partial(1/\tau_i)|$ at $\omega = \omega_0$, according to Eq. (A29). (b) $|a|^2/|s_{1+}|^2$ at $\omega = \omega_0$, according to Eq. (A30).

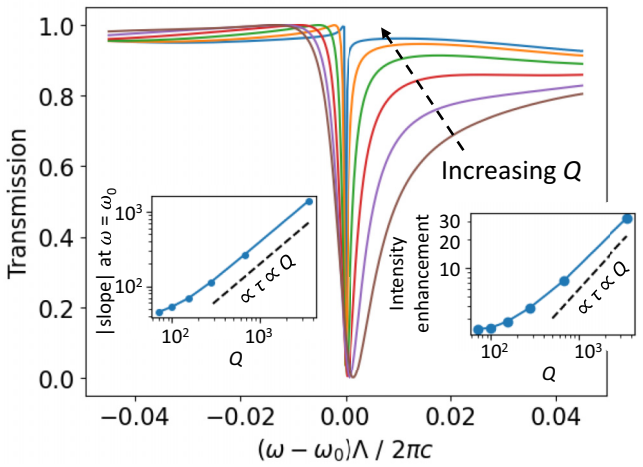

FIG. 6. Simulated transmission spectra with different values of Q, with the slopes at $\omega = \omega_0$ shown in the left inset and $\langle|E|^2\rangle$ at $\omega = \omega_0$ normalized by the counterpart evaluated for a bare silica surface shown in the right inset. Only the intensity in the solution region is taken into account in the right inset.

For the lossy structure, the field intensity of the resonant mode in Eq. (A27) becomes

$$|a|^2 = \frac{2|s_{1+}|^2/\tau_{e1}}{(\omega-\omega_0)^2 + (1/\tau_{e1}+1/\tau_{e2}+1/\tau_i)^2}, \tag{A30}$$

where the resonance decays into the two ports with rates $1/\tau_{e1}$ and $1/\tau_{e2}$, which satisfy $1/\tau_{e1} + 1/\tau_{e2} = 1/\tau_e$. In a regime in which τ_{e2}/τ_{e1} is nearly fixed as τ_e increases and $\max(\tau_{e1}, \tau_{e2}) \ll \tau_i$, the intensity is approximately proportional to $\tau_e \approx \tau$ or $Q_e \approx Q$ at $\omega = \omega_0$. As the example in Fig. 5(b) illustrates, for $\tau_e \ll \tau_i$, the normalized intensity $|a|^2/|s_{1+}|^2$ at $\omega = \omega_0$ scales linearly with τ_e or Q_e but approaches zero at $\tau_e \gg \tau_i$. Additionally, if τ_{e2}/τ_{e1} is not fixed but with $\tau_{e1} \ll \min(\tau_{e2}, \tau_{e1})$, the intensity is also approximately proportional to $\tau_{e1} \approx \tau_e \approx \tau$ or $Q_{e1} \approx Q_e \approx Q$ at $\omega = \omega_0$.

The simulation in the main text assumes no intrinsic loss. As shown in Fig. 6(a), the transmission spectra near $\omega = \omega_0$ steepen as $Q = Q_e$ increases. The slopes at $\omega = \omega_0$ scale asymptotically as Q, as illustrated in the inset. The simulated intensity enhancement, which also scales asymptotically as Q, is illustrated in Fig. 6(b).

APPENDIX B: GENERAL FRAMEWORK FOR MULTIPLICATIVE RESONANT ENHANCEMENT OF CHEMICAL DETECTION

In this appendix, we formulate a generalized framework to describe the multiplicative resonant enhancement effect for chemical detection.

Let us consider a more general reaction-diffusion system with a few assumptions. First, this system includes photochemical reactions with rate constants all proportional to the light intensity $I = |E|^2$ at a certain frequency, whereas all the other chemical species in this system do not respond to light and the relevant reaction rate constants are fixed and uniform in the reaction region. Second, in the regime of low light intensity and low concentration of the analyte, light can change the refractive index of the solution in the presence of the analyte but cannot in the absence of the analyte. Third, all the reactions are reversible. Fourth, the equilibrium concentrations $\mathbf{c}^{\mathrm{eq}}$ can be solved uniquely and described by a function of the intensity I and the analytical concentrations $\mathbf{c}^{\mathrm{an}}$ of all reagents including the analyte. The analytical concentration, also called the formal concentration, is the overall concentration of a substance regardless of its specific chemical forms or reactions that may happen when the solute is dissolved [20,21]. Let us write this relationship as

$$\mathbf{c}^{\mathrm{eq}} = f\left(\mathbf{c}^{\mathrm{an}}, I\right), \tag{B1}$$

where f denotes the function. At small I, one can expand Eq. (B1) in terms of I to first order, namely,

$$\mathbf{c}^{\mathrm{eq}} \approx f\left(\mathbf{c}^{\mathrm{an}}, I=0\right) + \left.\frac{\partial f}{\partial I}\right|_{I=0} I, \tag{B2}$$

where $f\left(\mathbf{c}^{\mathrm{an}}, I=0\right)$ computes the equilibrium concentrations in the dark. If the system is at equilibrium right before light turns on, $f\left(\mathbf{c}^{\mathrm{an}}, I=0\right)$ can be regarded as the initial concentrations (which need not be uniform in space):

$$f\left(\mathbf{c}^{\mathrm{an}}, I=0\right) = \mathbf{c}^{\mathrm{init}}. \tag{B3}$$

One can further expand $(\partial f/\partial I)|_{I=0}$ in terms of the analytical concentration of the analyte, denoted by c_x^{an}. The expansion to first order is

$$\left.\frac{\partial f}{\partial I}\right|_{I=0} \approx \left.\frac{\partial f}{\partial I}\right|_{I=c_x^{\mathrm{an}}=0} + \left.\frac{\partial^2 f}{\partial c_x^{\mathrm{an}} \partial I}\right|_{I=c_x^{\mathrm{an}}=0} c_x^{\mathrm{an}}. \tag{B4}$$

The difference between the initial and equilibrium concentrations, i.e., $\mathbf{c}^{\mathrm{eq}} - \mathbf{c}^{\mathrm{init}}$, can be obtained from Eqs. (B2)–(B4). Accordingly, the change of the refractive index is

$$\begin{aligned}\Delta n &= \mathbf{q}\cdot\left(\mathbf{c}^{\mathrm{eq}} - \mathbf{c}^{\mathrm{init}}\right) \\ &\approx \mathbf{q}\cdot\left.\frac{\partial f}{\partial I}\right|_{I=c_x^{\mathrm{an}}=0} I + \mathbf{q}\cdot\left.\frac{\partial^2 f}{\partial c_x^{\mathrm{an}}\partial I}\right|_{I=c_x^{\mathrm{an}}=0} I c_x^{\mathrm{an}},\end{aligned} \tag{B5}$$

where $\mathbf{q}$ is a vector that quantifies the linear change of the refractive index of the solution with respect to the change of the concentration of each solute. The first-derivative term here vanishes according to our assumption of no change in the refractive index in the absence of the analyte. If the second-derivative term does not vanish, one has $\Delta n \sim I c_x^{\mathrm{an}} \sim Q c_x^{\mathrm{an}}$.

The first-derivative term in Eq. (B5) vanishes in two typical scenarios. In the main text, the analyte is the only photoreactive species. Without the analyte, no photochemical reaction happens even in the presence of light, which implies that the first derivative in Eq. (B5) is zero. In the other scenario, the analyte is not a photoreactive species, or not the only photoreactive species in the system. The derivative $(\partial f/\partial I)|_{I=c_x^{\mathrm{an}}=0}$ itself may not be zero but, as in the example in Appendix C 2, some relations between physical parameters allow the combination $\mathbf{q}\cdot(\partial f/\partial I)|_{I=c_x^{\mathrm{an}}=0}$ to be zero.

If each photochemical reaction in this system is triggered by absorption of n photons with the same frequency, the reaction rate constant is proportional to I^n [14] and the intensity I in the above framework needs to be replaced by I^n, which enables Δn to scale asymptotically as $\sim Q^n$. Since the slope of the Fano-resonance line shape provides another enhancement factor of $\sim Q$, the detection sensitivity scales asymptotically as $\sim Q^{n+1}$.

In general, the substrate, grating, solvent, and solute can cause intrinsic losses. The scaling of sensitivity requires the intrinsic loss to be negligible compared to the loss due to radiative coupling. Chemical reactions may change the intrinsic loss. If the intrinsic loss is initially around zero but increases slightly as the reactions approach equilibrium, the scaling still holds, as implied by Eq. (A30) and the last expression in Eq. (A29), if the intrinsic loss is much smaller than the loss due to radiative coupling.

APPENDIX C: ANALYSIS OF CHEMICAL DETECTION WITH EXAMPLES

1. Chemical detection in a reaction-diffusion system with a single reversible reaction

In the model discussed in the main text, a closed system is assumed. At equilibrium, concentrations do not change with time and hence satisfy

$$\begin{aligned} D_0\nabla^2 c_0^{\mathrm{eq}} - k_0 c_0^{\mathrm{eq}} + k_1 c_1^{\mathrm{eq}} &= 0, \\ D_1\nabla^2 c_1^{\mathrm{eq}} + k_0 c_0^{\mathrm{eq}} - k_1 c_1^{\mathrm{eq}} &= 0. \end{aligned} \tag{C1}$$

In this appendix, equilibrium concentrations are labeled by the superscript eq, which is omitted in the main text. Cancelling the reaction terms in Eq. (C1), one can obtain

$$D_0\nabla^2 c_0^{\mathrm{eq}} + D_1\nabla^2 c_1^{\mathrm{eq}} = 0, \tag{C2}$$

which indicates that $D_0 c_0^{\mathrm{eq}} + D_1 c_1^{\mathrm{eq}}$ is uniform and hence satisfies

$$D_0 c_0^{\mathrm{eq}} + D_1 c_1^{\mathrm{eq}} = D_0\langle c_0^{\mathrm{eq}}\rangle + D_1\langle c_1^{\mathrm{eq}}\rangle. \tag{C3}$$

The angle brackets denote the average over the fluid, e.g.,

$$\langle c_0^{\mathrm{eq}}\rangle = \frac{1}{V}\int_\Omega c_0^{\mathrm{eq}} dv, \tag{C4}$$

where Ω is the fluid region with volume V and dv is the volume element in 3D or the area element in 2D. On the other hand, regardless of whether equilibrium is reached, material balance requires

$$\langle c_0\rangle + \langle c_1\rangle = \langle c\rangle, \tag{C5}$$

where $c = c_0|_{t=0}$ is the initial concentration of the reactant. Here, we assume that only the reactant, which is the analyte, is present in the beginning but this and subsequent equations are still correct if the product also exists at the start and c is changed as $c = c_0|_{t=0} + c_1|_{t=0}$. With Eqs. (C3) and (C5), one can find

$$c_0^{\mathrm{eq}} = \langle c\rangle + \left(\frac{D_1}{D_0} - 1\right)\langle c_1^{\mathrm{eq}}\rangle - \frac{D_1}{D_0}c_1^{\mathrm{eq}}. \tag{C6}$$

With Eqs. (C1) and (C6), one can cancel c_0 and obtain an integro-differential equation for c_1^{eq}:

$$\left[\frac{D_1}{D_0}k_0 + k_1 - D_1\nabla^2 + \left(1 - \frac{D_1}{D_0}\right)\frac{k_0}{V}\int_\Omega dv\cdot\right] c_1^{\mathrm{eq}} = k_0\langle c\rangle, \tag{C7}$$

where $\int_\Omega dv\cdot$ is understood as an operator for integration. The concentration at equilibrium can be formally written as

$$c_1^{\mathrm{eq}} = \left[\frac{D_1}{D_0}k_0 + k_1 - D_1\nabla^2 + \left(1 - \frac{D_1}{D_0}\right)\frac{k_0}{V}\int_\Omega dv\cdot\right]^{-1} k_0\langle c\rangle. \tag{C8}$$

The solution given by Eqs. (C6) and (C8) can be rewritten as

$$\begin{pmatrix} c_0^{\mathrm{eq}} \\ c_1^{\mathrm{eq}} \end{pmatrix} = \begin{bmatrix} 1 + \left(1 - \frac{D_1}{D_0}\right)\langle K^{-1}k_0\rangle - \frac{D_1}{D_0}K^{-1}k_0 \\ K^{-1}k_0 \end{bmatrix} c_0^{\mathrm{an}}, \tag{C9}$$

where $c_0^{\mathrm{an}} = \langle c\rangle$ is the analytical concentration of the reactant, which is also the analyte, and K denotes the operator in the square brackets of Eq. (C8). Using Eq. (C9), one can check that, without illumination, i.e., $k_0 = 0$, the equilibrium concentrations are $c_0^{\mathrm{eq}} = c_0^{\mathrm{an}}$ and $c_1^{\mathrm{eq}} = 0$. One can find the concentration change and hence the refractive-index change by starting with Eq. (C9) and then performing linearization in k_0. For demonstration purposes, however, here we continue the derivation in terms of the general framework of Appendix B.

The right-hand side of Eq. (C9) is the explicit form of the function f in Eq. (B1) for this reaction-diffusion system. For convenience, we use k_0 instead of I as the argument. Because of

$$\frac{\partial}{\partial k_0}\begin{pmatrix} c_0^{\mathrm{eq}} \\ c_1^{\mathrm{eq}} \end{pmatrix}\bigg|_{k_0 = c_0^{\mathrm{an}} = 0} = 0, \tag{C10}$$

the first-derivative term in Eq. (B5) equals zero. Because of

$$\frac{\partial^2}{\partial c_0^{\mathrm{an}}\partial k_0}\begin{pmatrix} c_0^{\mathrm{eq}} \\ c_1^{\mathrm{eq}} \end{pmatrix}\bigg|_{k_0 = c_0^{\mathrm{an}} = 0} k_0 c_0^{\mathrm{an}} = c_0^{\mathrm{an}}\begin{bmatrix} \left(1 - \frac{D_1}{D_0}\right)\langle K|_{k_0=0}^{-1}k_0\rangle - \frac{D_1}{D_0}K|_{k_0=0}^{-1}k_0 \\ K|_{k_0=0}^{-1}k_0 \end{bmatrix}, \tag{C11}$$

with $K|_{k_0=0}^{-1} = (k_1 - D_1\nabla^2)^{-1}$, the second-derivative term in Eq. (B5), i.e., the linearized change of the refractive index in this case, is

$$\begin{aligned}\Delta n &\approx \left(q_0 \frac{\partial^2 c_0^{\mathrm{eq}}}{\partial c_0^{\mathrm{an}} \partial k_0} + q_1 \frac{\partial^2 c_1^{\mathrm{eq}}}{\partial c_0^{\mathrm{an}} \partial k_0}\right)\Bigg|_{k_0 = c_0^{\mathrm{an}} = 0} k_0 c_0^{\mathrm{an}} \\ &= \left[\left(q_1 - q_0 \frac{D_1}{D_0}\right)(k_1 - D_1\nabla^2)^{-1} k_0 + q_0 \left(\frac{D_1}{D_0} - 1\right)\left\langle (k_1 - D_1\nabla^2)^{-1} k_0 \right\rangle\right] c_0^{\mathrm{an}}. \end{aligned} \tag{C12}$$

In this example, because the exact solution in Eq. (C9) is proportional to c_0^{an}, Eq. (C12) still holds if c_0^{an} is not small. For $k_0 \sim I$, Δn scales asymptotically as $\sim Q$. With another enhancement factor of $\sim Q$ from the slope of the Fano-resonance line shape, the detection sensitivity scales asymptotically as $\sim Q^2$. In the main text, we additionally assume $D_0 = D_1$, which allows further simplification.

In our simulation, because of the silicon nitride ridges, the effective reaction vessel is not rectangular. To solve for the equilibrium concentration and change of the refractive index in such a region, we enclose the solution region plus the grating in a rectangular computational cell and write the diffusion term in its general form, i.e., $\nabla \cdot (D\nabla)$ with $D = \rho D_i$, where D_i is a diffusion coefficient in the fluid and ρ varies between 1 and 0, with $\rho = 1$ in the fluid region and $\rho = 0$ in the region occupied by the ridges. On the lateral boundaries between ridges and solution, ρ can take intermediate values between 0 and 1.

2. Chemical detection in a reaction-diffusion system with two coupled reversible reactions

In this section, we consider two coupled reversible reactions as

$$\mathrm{A} \underset{}{\overset{h\nu}{\rightleftharpoons}} \mathrm{A}^*, \qquad \mathrm{A}^* + \mathrm{X} \rightleftharpoons \mathrm{AX}, \tag{C13}$$

where the forward process in the former reaction is induced by light while all the other processes are not. As a typical scenario, all chemicals are assumed to be dissolved in solvent, which may be liquid or gaseous, in a closed system. The target being detected, namely, the analyte, is X. Before light turns on, only A and X are present; after light turns on, the concentrations of the four chemical species evolve with time t according to a set of reaction-diffusion equations:

$$\begin{aligned}\frac{\partial c_{\mathrm{A}}}{\partial t} &= D_{\mathrm{A}}\nabla^2 c_{\mathrm{A}} - k_{\mathrm{act}} c_{\mathrm{A}} + k_{\mathrm{deact}} c_*, \\ \frac{\partial c_*}{\partial t} &= D_*\nabla^2 c_* + k_{\mathrm{act}} c_{\mathrm{A}} - k_{\mathrm{deact}} c_* - k_{\mathrm{com}} c_* c_{\mathrm{X}} + k_{\mathrm{decom}} c_{\mathrm{AX}}, \\ \frac{\partial c_{\mathrm{X}}}{\partial t} &= D_{\mathrm{X}}\nabla^2 c_{\mathrm{X}} - k_{\mathrm{com}} c_* c_{\mathrm{X}} + k_{\mathrm{decom}} c_{\mathrm{AX}}, \\ \frac{\partial c_{\mathrm{AX}}}{\partial t} &= D_{\mathrm{AX}}\nabla^2 c_{\mathrm{AX}} + k_{\mathrm{com}} c_* c_{\mathrm{X}} - k_{\mathrm{decom}} c_{\mathrm{AX}}. \end{aligned} \tag{C14}$$

where c_{A}, c_*, c_{X}, and c_{AX} denote the concentrations of A, A*, X, and AX, respectively, and the corresponding diffusion coefficients are denoted as D_{A}, D_*, D_{X}, and D_{AX}. In the first reaction in Eq. (C13), the species A is activated by light and becomes A* with the activation rate constant k_{act}. The deactivation process from A* to A occurs with the rate constant k_{deact}. In the second reaction, A* combines reversibly with the target species X. The rate constants of combination and decomposition are denoted by k_{com} and k_{decom}, respectively. Among all these diffusion coefficients and rate constants, only k_{act} depends on light and can be nonuniform.

At equilibrium, all time derivatives in Eq. (C14) vanish. Taking total derivatives on the resultant equations, one can obtain

$$\begin{aligned} 0 &= (D_{\mathrm{A}}\nabla^2 - k_{\mathrm{act}}) dc_{\mathrm{A}}^{\mathrm{eq}} + k_{\mathrm{deact}} dc_*^{\mathrm{eq}} - c_{\mathrm{A}}^{\mathrm{eq}} dk_{\mathrm{act}}, \\ 0 &= k_{\mathrm{act}} dc_{\mathrm{A}}^{\mathrm{eq}} + (D_*\nabla^2 - k_{\mathrm{com}} c_{\mathrm{X}}^{\mathrm{eq}} - k_{\mathrm{deact}}) dc_*^{\mathrm{eq}} - k_{\mathrm{com}} c_*^{\mathrm{eq}} dc_{\mathrm{X}}^{\mathrm{eq}} + k_{\mathrm{decom}} dc_{\mathrm{AX}}^{\mathrm{eq}} + c_{\mathrm{A}}^{\mathrm{eq}} dk_{\mathrm{act}}, \\ 0 &= -k_{\mathrm{com}} c_{\mathrm{X}}^{\mathrm{eq}} dc_*^{\mathrm{eq}} + (D_{\mathrm{X}}\nabla^2 - k_{\mathrm{com}} c_*^{\mathrm{eq}}) dc_{\mathrm{X}}^{\mathrm{eq}} + k_{\mathrm{decom}} dc_{\mathrm{AX}}^{\mathrm{eq}}, \\ 0 &= k_{\mathrm{com}} c_{\mathrm{X}}^{\mathrm{eq}} dc_*^{\mathrm{eq}} + k_{\mathrm{com}} c_*^{\mathrm{eq}} dc_{\mathrm{X}}^{\mathrm{eq}} + (D_{\mathrm{AX}}\nabla^2 - k_{\mathrm{decom}}) dc_{\mathrm{AX}}^{\mathrm{eq}}. \end{aligned} \tag{C15}$$

In the dark, the system satisfies

$$k_{\mathrm{act}} = c_{*}^{\mathrm{eq}} = c_{\mathrm{AX}}^{\mathrm{eq}} = 0, \quad c_{\mathrm{A}}^{\mathrm{eq}} = c_{\mathrm{A}}^{\mathrm{an}}, \quad c_{\mathrm{X}}^{\mathrm{eq}} = c_{\mathrm{X}}^{\mathrm{an}}, \tag{C16}$$

where $c_{\mathrm{A}}^{\mathrm{an}}$ and $c_{\mathrm{X}}^{\mathrm{an}}$ denote the analytical concentrations of A and X. From Eqs. (C15) and (C16) one can obtain

$$\begin{aligned}
\left.\frac{\partial c_{\mathrm{AX}}^{\mathrm{eq}}}{\partial k_{\mathrm{act}}}\right|_{k_{\mathrm{act}}=0} &= k_{\mathrm{com}} c_{\mathrm{A}}^{\mathrm{an}} c_{\mathrm{X}}^{\mathrm{an}} \left[D_{*} D_{\mathrm{AX}} \nabla^2 \nabla^2 \right. \\
&\quad \left. -(D_{\mathrm{AX}} k_{\mathrm{com}} c_{\mathrm{X}}^{\mathrm{an}} + D_{*} k_{\mathrm{decom}}) \nabla^2 + k_{\mathrm{deact}} k_{\mathrm{decom}}\right]^{-1}, \\
\left.\frac{\partial c_{*}^{\mathrm{eq}}}{\partial k_{\mathrm{act}}}\right|_{k_{\mathrm{act}}=0} &= \frac{k_{\mathrm{decom}} - D_{\mathrm{AX}} \nabla^2}{k_{\mathrm{com}} c_{\mathrm{X}}^{\mathrm{an}}} \left.\frac{\partial c_{\mathrm{AX}}^{\mathrm{eq}}}{\partial k_{\mathrm{act}}}\right|_{k_{\mathrm{act}}=0} \\
&= c_{\mathrm{A}}^{\mathrm{an}} (k_{\mathrm{decom}} - D_{\mathrm{AX}} \nabla^2) \cdot \left[D_{*} D_{\mathrm{AX}} \nabla^2 \nabla^2 \right. \\
&\quad \left. -(D_{\mathrm{AX}} k_{\mathrm{com}} c_{\mathrm{X}}^{\mathrm{an}} + D_{*} k_{\mathrm{decom}}) \nabla^2 + k_{\mathrm{deact}} k_{\mathrm{decom}}\right]^{-1}.
\end{aligned} \tag{C17}$$

Solving for the gradients of $c_{\mathrm{A}}^{\mathrm{eq}}$ and $c_{\mathrm{X}}^{\mathrm{eq}}$ involves additional steps. First, similar to Eqs. (C2) and (C3), by canceling reaction terms in the equilibrium equations, one can obtain

$$D_{\mathrm{A}} \nabla^2 c_{\mathrm{A}}^{\mathrm{eq}} + D_{*} \nabla^2 c_{*}^{\mathrm{eq}} + D_{\mathrm{AX}} \nabla^2 c_{\mathrm{AX}}^{\mathrm{eq}} = D_{\mathrm{X}} \nabla^2 c_{\mathrm{X}}^{\mathrm{eq}} + D_{\mathrm{AX}} \nabla^2 c_{\mathrm{AX}}^{\mathrm{eq}} = 0, \tag{C18}$$

which indicates that $D_{\mathrm{A}} c_{\mathrm{A}}^{\mathrm{eq}} + D_{*} c_{*}^{\mathrm{eq}} + D_{\mathrm{AX}} c_{\mathrm{AX}}^{\mathrm{eq}}$ and $D_{\mathrm{X}} c_{\mathrm{X}}^{\mathrm{eq}} + D_{\mathrm{AX}} c_{\mathrm{AX}}^{\mathrm{eq}}$ do not vary over space in the fluid region and hence satisfy

$$\begin{aligned}
D_{\mathrm{A}} c_{\mathrm{A}}^{\mathrm{eq}} + D_{*} c_{*}^{\mathrm{eq}} + D_{\mathrm{AX}} c_{\mathrm{AX}}^{\mathrm{eq}} &= D_{\mathrm{A}} \langle c_{\mathrm{A}}^{\mathrm{eq}} \rangle + D_{*} \langle c_{*}^{\mathrm{eq}} \rangle + D_{\mathrm{AX}} \langle c_{\mathrm{AX}}^{\mathrm{eq}} \rangle, \\
D_{\mathrm{X}} c_{\mathrm{X}}^{\mathrm{eq}} + D_{\mathrm{AX}} c_{\mathrm{AX}}^{\mathrm{eq}} &= D_{\mathrm{X}} \langle c_{\mathrm{X}}^{\mathrm{eq}} \rangle + D_{\mathrm{AX}} \langle c_{\mathrm{AX}}^{\mathrm{eq}} \rangle.
\end{aligned} \tag{C19}$$

On the other hand, material balance requires

$$c_{\mathrm{A}}^{\mathrm{an}} = \langle c_{\mathrm{A}} \rangle + \langle c_{*} \rangle + \langle c_{\mathrm{AX}} \rangle, \quad c_{\mathrm{X}}^{\mathrm{an}} = \langle c_{\mathrm{X}} \rangle + \langle c_{\mathrm{AX}} \rangle. \tag{C20}$$

From Eqs. (C19) and (C20), one can find

$$\begin{aligned}
\left.\frac{\partial c_{\mathrm{A}}^{\mathrm{eq}}}{\partial k_{\mathrm{act}}}\right|_{k_{\mathrm{act}}=0} &= \left(\frac{D_{\mathrm{AX}}}{D_{\mathrm{A}}} - 1\right) \left\langle \frac{\partial c_{\mathrm{AX}}^{\mathrm{eq}}}{\partial k_{\mathrm{act}}} \right\rangle \Bigg|_{k_{\mathrm{act}}=0} - \frac{D_{\mathrm{AX}}}{D_{\mathrm{A}}} \left.\frac{\partial c_{\mathrm{AX}}^{\mathrm{eq}}}{\partial k_{\mathrm{act}}}\right|_{k_{\mathrm{act}}=0} \\
&\quad + \left(\frac{D_{*}}{D_{\mathrm{A}}} - 1\right) \left\langle \frac{\partial c_{*}^{\mathrm{eq}}}{\partial k_{\mathrm{act}}} \right\rangle \Bigg|_{k_{\mathrm{act}}=0} - \frac{D_{*}}{D_{\mathrm{A}}} \left.\frac{\partial c_{*}^{\mathrm{eq}}}{\partial k_{\mathrm{act}}}\right|_{k_{\mathrm{act}}=0}, \\
\left.\frac{\partial c_{\mathrm{X}}^{\mathrm{eq}}}{\partial k_{\mathrm{act}}}\right|_{k_{\mathrm{act}}=0} &= \left(\frac{D_{\mathrm{AX}}}{D_{\mathrm{X}}} - 1\right) \left\langle \frac{\partial c_{\mathrm{AX}}^{\mathrm{eq}}}{\partial k_{\mathrm{act}}} \right\rangle \Bigg|_{k_{\mathrm{act}}=0} - \frac{D_{\mathrm{AX}}}{D_{\mathrm{X}}} \left.\frac{\partial c_{\mathrm{AX}}^{\mathrm{eq}}}{\partial k_{\mathrm{act}}}\right|_{k_{\mathrm{act}}=0}.
\end{aligned} \tag{C21}$$

In Eqs. (C17) and (C21), only the first derivative of $c_{\mathrm{A}}^{\mathrm{eq}}$ and c_{*}^{eq} survives at $c_{\mathrm{X}}^{\mathrm{an}} = 0$. Therefore, the first-derivative term in Eq. (B5) is

$$\begin{aligned}
&\left(q_{\mathrm{A}} \frac{\partial c_{\mathrm{A}}^{\mathrm{eq}}}{\partial k_{\mathrm{act}}} + q_{*} \frac{\partial c_{*}^{\mathrm{eq}}}{\partial k_{\mathrm{act}}} + q_{\mathrm{X}} \frac{\partial c_{\mathrm{X}}^{\mathrm{eq}}}{\partial k_{\mathrm{act}}} + q_{\mathrm{AX}} \frac{\partial c_{\mathrm{AX}}^{\mathrm{eq}}}{\partial k_{\mathrm{act}}}\right)\Bigg|_{k_{\mathrm{act}}=c_{\mathrm{X}}^{\mathrm{an}}=0} \\
&= q_{\mathrm{A}} \left(\frac{D_{*}}{D_{\mathrm{A}}} - 1\right) \left\langle \frac{\partial c_{*}^{\mathrm{eq}}}{\partial k_{\mathrm{act}}} \right\rangle \Bigg|_{k_{\mathrm{act}}=c_{\mathrm{X}}^{\mathrm{an}}=0} + \left(q_{*} - q_{\mathrm{A}} \frac{D_{*}}{D_{\mathrm{A}}}\right) \left.\frac{\partial c_{*}^{\mathrm{eq}}}{\partial k_{\mathrm{act}}}\right|_{k_{\mathrm{act}}=c_{\mathrm{X}}^{\mathrm{an}}=0},
\end{aligned} \tag{C22}$$

where q_i (i = A, A*, X, and AX) quantifies the linear change of the refractive index of the solution with respect to the change of the concentration of each solute. We assume that the structures of A and A* are nearly the same, so that the two species have

$$D_{\mathrm{A}} = D_*, \quad q_{\mathrm{A}} = q_*. \tag{C23}$$

Under this condition, the first-derivative term in Eq. (B5), i.e., Eq. (C22) in this example, vanishes. Using Eqs. (C17), (C21), and (C23), one can also obtain

$$\begin{aligned}
&\left(q_{\mathrm{A}}\frac{\partial^2 c_{\mathrm{A}}^{\mathrm{eq}}}{\partial k_{\mathrm{act}}} + q_*\frac{\partial^2 c_*^{\mathrm{eq}}}{\partial k_{\mathrm{act}}} + q_{\mathrm{X}}\frac{\partial^2 c_{\mathrm{X}}^{\mathrm{eq}}}{\partial k_{\mathrm{act}}} + q_{\mathrm{AX}}\frac{\partial^2 c_{\mathrm{AX}}^{\mathrm{eq}}}{\partial k_{\mathrm{act}}}\right)\Big|_{k_{\mathrm{act}}=0} \\
&= \left\{\left(q_{\mathrm{AX}} - q_{\mathrm{A}}\frac{D_{\mathrm{AX}}}{D_{\mathrm{A}}} - q_{\mathrm{X}}\frac{D_{\mathrm{AX}}}{D_{\mathrm{X}}}\right)\frac{\partial c_{\mathrm{AX}}^{\mathrm{eq}}}{\partial k_{\mathrm{act}}} + \left(q_* - q_{\mathrm{A}}\frac{D_*}{D_{\mathrm{A}}}\right)\frac{\partial c_*^{\mathrm{eq}}}{\partial k_{\mathrm{act}}}\right. \\
&\quad \left. + \left[q_{\mathrm{A}}\left(\frac{D_{\mathrm{AX}}}{D_{\mathrm{A}}} - 1\right) + q_{\mathrm{X}}\left(\frac{D_{\mathrm{AX}}}{D_{\mathrm{X}}} - 1\right)\right]\left\langle\frac{\partial c_{\mathrm{AX}}^{\mathrm{eq}}}{\partial k_{\mathrm{act}}}\right\rangle + q_{\mathrm{A}}\left(\frac{D_*}{D_{\mathrm{A}}} - 1\right)\left\langle\frac{\partial c_*^{\mathrm{eq}}}{\partial k_{\mathrm{act}}}\right\rangle\right\}_{k_{\mathrm{act}}=0} \\
&= \left\{\left(q_{\mathrm{AX}} - q_{\mathrm{A}}\frac{D_{\mathrm{AX}}}{D_{\mathrm{A}}} - q_{\mathrm{X}}\frac{D_{\mathrm{AX}}}{D_{\mathrm{X}}}\right)\frac{\partial c_{\mathrm{AX}}^{\mathrm{eq}}}{\partial k_{\mathrm{act}}} + \left[q_{\mathrm{A}}\left(\frac{D_{\mathrm{AX}}}{D_{\mathrm{A}}} - 1\right) + q_{\mathrm{X}}\left(\frac{D_{\mathrm{AX}}}{D_{\mathrm{X}}} - 1\right)\right]\left\langle\frac{\partial c_{\mathrm{AX}}^{\mathrm{eq}}}{\partial k_{\mathrm{act}}}\right\rangle\right\}_{k_{\mathrm{act}}=0}.
\end{aligned} \tag{C24}$$

The second-derivative term in Eq. (B5), which is the lowest-order change of the refractive index in this example, can then be written as

$$\begin{aligned}
\Delta n &\approx \left(q_{\mathrm{A}}\frac{\partial^2 c_{\mathrm{A}}^{\mathrm{eq}}}{\partial c_{\mathrm{X}}^{\mathrm{an}}\partial k_{\mathrm{act}}} + q_*\frac{\partial^2 c_*^{\mathrm{eq}}}{\partial c_{\mathrm{X}}^{\mathrm{an}}\partial k_{\mathrm{act}}} + q_{\mathrm{X}}\frac{\partial^2 c_{\mathrm{X}}^{\mathrm{eq}}}{\partial c_{\mathrm{X}}^{\mathrm{an}}\partial k_{\mathrm{act}}} + q_{\mathrm{AX}}\frac{\partial^2 c_{\mathrm{AX}}^{\mathrm{eq}}}{\partial c_{\mathrm{X}}^{\mathrm{an}}\partial k_{\mathrm{act}}}\right)\Big|_{k_{\mathrm{act}}=c_{\mathrm{X}}^{\mathrm{an}}=0} k_{\mathrm{act}}c_{\mathrm{X}}^{\mathrm{an}} \\
&= k_{\mathrm{com}}c_{\mathrm{A}}^{\mathrm{an}}c_{\mathrm{X}}^{\mathrm{an}}\left\{\left(q_{\mathrm{AX}} - q_{\mathrm{A}}\frac{D_{\mathrm{AX}}}{D_{\mathrm{A}}} - q_{\mathrm{X}}\frac{D_{\mathrm{AX}}}{D_{\mathrm{X}}}\right)L^{-1}k_{\mathrm{act}} + \left[q_{\mathrm{A}}\left(\frac{D_{\mathrm{AX}}}{D_{\mathrm{A}}} - 1\right) + q_{\mathrm{X}}\left(\frac{D_{\mathrm{AX}}}{D_{\mathrm{X}}} - 1\right)\right]\langle L^{-1}k_{\mathrm{act}}\rangle\right\},
\end{aligned} \tag{C25}$$

with

$$L = D_*D_{\mathrm{AX}}\nabla^2\nabla^2 - D_*k_{\mathrm{decom}}\nabla^2 + k_{\mathrm{deact}}k_{\mathrm{decom}}. \tag{C26}$$

For $k_{\mathrm{act}} \sim I$, Δn scales asymptotically as $\sim Q$. With another enhancement factor of $\sim Q$ from the slope of the Fano-resonance line shape, the detection sensitivity scales asymptotically as $\sim Q^2$.

[1] J. D. Jackson, *Classical Electrodynamics* (John Wiley & Sons, New York, 1998), 3rd ed.

[2] B. E. A. Saleh and M. C. Teich, *Fundamentals of Photonics* (John Wiley & Sons, New York, 2019), 3rd ed.

[3] J. Homola, Surface plasmon resonance sensors for detection of chemical and biological species, Chem. Rev. **108**, 462 (2008).

[4] M. S. Luchansky and R. C. Bailey, High-Q optical sensors for chemical and biological analysis, Anal. Chem. **84**, 793 (2011).

[5] G. Gagliardi and H.-P. Loock, in *Springer Series in Optical Sciences 179* (Springer, Berlin, 2014).

[6] G. Pitruzzello and T. F. Krauss, Photonic crystal resonances for sensing and imaging, J. Opt. **20**, 073004 (2018).

[7] D. Yu, M. Humar, K. Meserve, R. C. Bailey, S. N. Chormaic, and F. Vollmer, Whispering-gallery-mode sensors for biological and physical sensing, Nat. Rev. Methods Primers **1**, 83 (2021).

[8] A. K. Ray and D. D. Bhanti, Effect of optical resonances on photochemical reactions in microdroplets, Appl. Opt. **36**, 2663 (1997).

[9] P. Corral Arroyo, G. David, P. A. Alpert, E. A. Parmentier, M. Ammann, and R. Signorell, Amplification of light within aerosol particles accelerates in-particle photochemistry, Science **376**, 293 (2022).

[10] S. Fan, W. Suh, and J. D. Joannopoulos, Temporal coupled-mode theory for the Fano resonance in optical resonators, J. Opt. Soc. Am. A **20**, 569 (2003).

[11] J. D. Joannopoulos, S. G. Johnson, J. N. Winn, and R. D. Meade, *Photonic Crystals: Molding the Flow of Light* (Princeton University Press, Princeton, 2008), 2nd ed.

[12] P. Lalanne, W. Yan, K. Vynck, C. Sauvan, and J. Hugonin, Light interaction with photonic and plasmonic resonances, Laser Photonics Rev. **12**, 1700113 (2018).

[13] D. M. Pozar, *Microwave Engineering* (John Wiley & Sons, Hoboken, 2012), 4th ed.

[14] R. W. Boyd, *Nonlinear Optics* (Academic Press, Elsevier, New York, 2020), 4th ed.

[15] E. C. L. Ru and P. G. Etchegoin, *Principles of Surface-Enhanced Raman Spectroscopy* (Elsevier, Amsterdam, 2011).

[16] T. P. Pearsall, *Quantum Photonics* (Springer, Berlin, 2018).

[17] C.-Y. Tan and Y.-X. Huang, Dependence of refractive index on concentration and temperature in electrolyte solution,

polar solution, nonpolar solution, and protein solution, J. Chem. Eng. Data **60**, 2827 (2015).
[18] T. G. Mayerhöfer, A. Dabrowska, A. Schwaighofer, B. Lendl, and J. Popp, Beyond Beer's law: Why the index of refraction depends (almost) linearly on concentration, ChemPhysChem **21**, 707 (2020).
[19] P. W. Atkins, D. J. Paula, and J. Keeler, *Atkins' Physical Chemistry* (Oxford University Press, Oxford, 2023), 11th ed.
[20] D. C. Harris, *Quantitative Chemical Analysis* (W. H. Freeman and Company, New York, 2010), 8th ed.
[21] D. A. Skoog, D. M. West, F. J. Holler, and S. R. Crouch, *Fundamentals of Analytical Chemistry* (Cengage, Boston, 2021), 10th ed.
[22] Y. Guo, J. Y. Ye, C. Divin, B. Huang, T. P. Thomas, J. R. Baker Jr, and T. B. Norris, Real-time biomolecular binding detection using a sensitive photonic crystal biosensor, Anal. Chem. **82**, 5211 (2010).
[23] X. Fan and I. M. White, Optofluidic microsystems for chemical and biological analysis, Nat. Photonics **5**, 591 (2011).
[24] A. H. Aly, S. K. Awasthi, D. Mohamed, Z. S. Matar, M. Al-Dossari, and A. F. Amin, Study on a one-dimensional defective photonic crystal suitable for organic compound sensing applications, RSC Adv. **11**, 32973 (2021).
[25] W. Suh, Z. Wang, and S. Fan, Temporal coupled-mode theory and the presence of non-orthogonal modes in lossless multimode cavities, IEEE J. Quantum Electron. **40**, 1511 (2004).
[26] Z. Zhao, C. Guo, and S. Fan, Connection of temporal coupled-mode-theory formalisms for a resonant optical system and its time-reversal conjugate, Phys. Rev. A **99**, 033839 (2019).
[27] T. Christopoulos, O. Tsilipakos, and E. E. Kriezis, Temporal coupled-mode theory in nonlinear resonant photonics: From basic principles to contemporary systems with 2D materials, dispersion, loss, and gain, J. Appl. Phys. **136**, 011101 (2024).
[28] A. C. Overvig, S. Shrestha, and N. Yu, Dimerized high contrast gratings, Nanophotonics **7**, 1157 (2018).
[29] C. W. Hsu, B. Zhen, J. Lee, S.-L. Chua, S. G. Johnson, J. D. Joannopoulos, and M. Soljačić, Observation of trapped light within the radiation continuum, Nature **499**, 188 (2013).
[30] C. W. Hsu, B. Zhen, A. D. Stone, J. D. Joannopoulos, and M. Soljačić, Bound states in the continuum, Nat. Rev. Mater. **1**, 16048 (2016).
[31] S. G. Johnson and J. D. Joannopoulos, Block-iterative frequency-domain methods for Maxwell's equations in a planewave basis, Opt. Express **8**, 173 (2001).
[32] K. Koshelev, S. Lepeshov, M. Liu, A. Bogdanov, and Y. Kivshar, Asymmetric metasurfaces with high-resonances governed by bound states in the continuum, Phys. Rev. Lett. **121**, 193903 (2018).
[33] S. G. Johnson, M. L. Povinelli, M. Soljačić, A. Karalis, S. Jacobs, and J. D. Joannopoulos, Roughness losses and volume-current methods in photonic-crystal waveguides, Appl. Phys. B **81**, 283 (2005).
[34] A. F. Oskooi, D. Roundy, M. Ibanescu, P. Bermel, J. D. Joannopoulos, and S. G. Johnson, MEEP: A flexible free-software package for electromagnetic simulations by the FDTD method, Comput. Phys. Commun. **181**, 687 (2010).
[35] K. X. Wang, Z. Yu, S. Sandhu, and S. Fan, Fundamental bounds on decay rates in asymmetric single-mode optical resonators, Opt. Lett. **38**, 100 (2013).
[36] H.-G. Beyer, *The Theory of Evolution Strategies* (Springer, Berlin, 2001).
[37] P. Klán and J. Wirz, *Photochemistry of Organic Compounds: From Concepts to Practice* (John Wiley and Sons, Chichester, 2010).
[38] A. Zanutta, L. Colella, C. Bertarelli, and A. Bianco, Understanding the mechanism of refractive index modulation in materials undergoing photo-Fries rearrangement, Opt. Mater. **35**, 2283 (2013).
[39] H. Zhao, J. Sha, X. Wang, Y. Jiang, T. Chen, T. Wu, X. Chen, H. Ji, Y. Gao, L. Xie, and Y. Ma, Spatiotemporal control of polymer brush formation through photoinduced radical polymerization regulated by DMD light modulation, Lab Chip **19**, 2651 (2019).
[40] H. Kudo, M. Yamamoto, and T. Nishikubo, Refractive index change during photo crosslinking reaction of poly (silsesquioxane) derivatives containing cinnamoyl moieties in the side chains, J. Network Polym. Jpn. **28**, 11 (2007).
[41] H. Kudo, M. Yamamoto, T. Nishikubo, and O. Moriya, Novel materials for large change in refractive index: Synthesis and photochemical reaction of the ladderlike poly(silsesquioxane) containing norbornadiene, azobenzene, and anthracene groups in the side chains, Macromolecules **39**, 1759 (2006).
[42] M. D. Cohen, The photochemistry of organic solids, Angew. Chem. Int. Ed. Engl. **14**, 386 (1975).
[43] J. M. Cole and M. Irie, Solid-state photochemistry, CrystEngComm **18**, 7175 (2016).
[44] M. Soljačić, M. Ibanescu, S. G. Johnson, Y. Fink, and J. D. Joannopoulos, Optimal bistable switching in nonlinear photonic crystals, Phys. Rev. E **66**, 055601 (2002).
[45] N. G. Greeneltch, M. G. Blaber, G. C. Schatz, and R. P. Van Duyne, Plasmon-sampled surface-enhanced Raman excitation spectroscopy on silver immobilized nanorod assemblies and optimization for near infrared ($\lambda_{ex} = 1064$ nm) studies, J. Phys. Chem. C **117**, 2554 (2013).
[46] M. Mohammadi, M. Farahmand, S. Olyaee, and M. Seifouri, An overview of all-optical memories based on periodic structures used in integrated optical circuits, Silicon **14**, 8661 (2022).
[47] P. L. Stiles, J. A. Dieringer, N. C. Shah, and R. P. Van Duyne, Surface-enhanced Raman spectroscopy, Annu. Rev. Anal. Chem. **1**, 601 (2008).
[48] R. Pilot, R. Signorini, C. Durante, L. Orian, M. Bhamidipati, and L. Fabris, A review on surface-enhanced Raman scattering, Biosensors **9**, 57 (2019).
[49] J. Langer, *et al.*, Present and future of surface-enhanced Raman scattering, ACS Nano **14**, 28 (2019).